Computation of flexoelectric coefficients of a MoS2 monolayer with a model of self-consistently distributed effective charges and dipoles

Yida Yang, Laurent Hirsinger, Michel Devel

Computation of Flexoelectric Coefficients of a MoS_2 monolayer with a Model of Self-consistently Distributed Effective Charges and Dipoles

Yida Yang,[1] Laurent Hirsinger,[1] and Michel Devel[1,*]

[1]*FEMTO-ST institute, UBFC, CNRS, ENSMM, 15B avenue des Montboucons, 25030 Besançon CEDEX, France*

Abstract

Flexoelectricity is an electromechanical coupling phenomenon, that can generate noticeable electric polarization in dielectric materials for nanoscale strain gradients. It is gaining an increasing attention because of its potential applications, and the fact that experimental results were initially an order of magnitude higher than initial theoretical predictions. This stimulated intense experimental and theoretical researches to investigate flexoelectric coefficients in dielectric materials such as two-dimensional materials. In this work, we concentrate on the calculation of the flexoelectric coefficients of 2D-MoS_2 thanks to a model using self-consistently determined charges and dipoles on the atoms. More specifically, we study the importance of two contributions which were neglected/omitted in previous papers using this model, namely the charge term in the total polarization and the conservation of electric charge through a Lagrange multiplier. Our calculations demonstrate that the results for flexoelectric coefficient computed with this improved definition of polarization agree better with experimental measurements, provided consistent definitions for signs are used. Additionally, we show how two physical contributions with opposite signs compete to give net values of flexoelectric coefficients that can be either positive or negative depending on their relative importance, and give net values for the case of MoS_2.

*Electronic address: michel.devel@femto-st.fr

I. INTRODUCTION

Flexoelectricity[1], a fascinating electromechanical phenomenon, is widely employed to describe electric polarization caused by strain gradient. Unlike piezoelectricity, which arises only in noncentrosymmetric materials, flexoelectricity can a priori exist in all materials. Therefore, flexoelectricity can provide new opportunities to use some centrosymmetric materials to build electromechanical systems, such as energy harvesters[2, 3], actuators[4, 5], flexible electronics[6], flexoelectric sensors[7, 8].

Flexoelectricity was first predicted by Mashkevich and Tolpygo[9] during Tolpygo's studies on the optical and elastic properties of crystals. The polarization due to the flexoelectric effect was later phenomenologically described by Kogan[10], using the contraction of a fourth order flexoelectricity tensor with the third order strain gradient tensor. Ever since the terminology 'flexoelectricity' was firstly borrowed from the liquid crystals community by Indenbom[11, 12] et al in 1981, a great deal of theoretical work has been done to advance the development of the theory of flexoelectricity in solids. Earlier theoretical descriptions principally concentrated on lattice dynamics using Kogan's phenomenological theory[10, 13, 14] and continuum mechanics[15] or microscopic theories based on lattice dynamics[13, 16–18] and quantum mechanics[19–22]. Calculations used methods such as core-shell model[17, 23], rigid-ion model[13, 14], molecular dynamics simulations[24–26], finite element method[27, 28] and phase-field method[29]. Recently, the advancement and popularity of machine learning techniques[30–32] provide original means for the computation of flexoelectricity coefficients. A novel technique called topology optimization methods have been proposed allowing for more accurate and efficient design of complex flexoelectric structures[33]. Another strategy, the isogeometric analysis (IGA), which fulfills the C1-continuity requirement has been adopted to identify the full flexoelectric properties based on electrical impedance curves.[34]

Flexoelectricity in solids was believed to be a very small effect. However, at the beginning of the 2000s, Ma and Cross reported unexpectedly high experimental flexoelectric responses in a variety of perovskite ceramics [35–40] greatly arousing the interest in research of flexoelectricity in perovskite ceramics.[41–43] Furthermore, the relative importance of the flexoelectric effect with respect to the piezoelectric effect should increase as the scale of strain inhomogeneities decreases. Therefore, the recent development of ultrathin (2D) nanomaterials, due to the desired need for miniaturized devices, provide opportunities for researchers to study flexoelectricity in 2D materials which could offer interesting electromechanical coupling in nanodevices. Such an interest has stimulated intense research to investigate flexoelectric coefficients in carbon nanomaterials[20, 21, 44–46] (nanotubes, fullerenes, nanocores and patterned graphene), phosphorene[47], hexagonal boron nitride[48] and transition-metal dichalcogenides[49, 50] by means of first-principle calculations. Remarkably, Kumar et al very recently calculated the flexoelectric coefficient for fifty-four representative atomic monolayers selected from distinct groups in the periodic table of elements using ab-initio Density Functional Theory (DFT)[51].

Recently, Zhuang and co-workers used molecular dynamics simulations coupled with a charge dipole (QP) model to compute flexoelectric coefficients for transition-metal dichalcogenides[52] and related materials[53]. This kind of method uses calculations much faster than DFT calculations, and provides an easier way to predict the properties of bigger and less symmetric heterostructures. Since we have some experience in using the QP model[54–56] we studied those papers in details and noticed that a term involving effective charges was neglected/omitted in the definition of polarization that only used the effective dipoles, as in the case of covalent materials such as e.g. graphene. Furthermore, the enforcement of charge conservation was also not implemented, meaning that charges could flow in or out of the materials without any constraint, which can conflict with the fact that an

insulating substrate (Polydimethylsiloxane (PDMS), Au, Al_2O_3)[57, 58] was used to obtain the out-of-plane effective flexoelectricity coefficient of monolayer MoS_2, by using an equation for converse flexoelectricity to link the out-of-plane effective piezoelectric coefficient measured by piezoresponse force microscopy and the flexoelectric coefficient to be determined[57, 58]. We also note that in-plane flexoelectric coefficients μ_{1111} or μ_{2222} for such 2D materials have not yet been experimentally obtained, since it has been difficult to isolate the relative contributions of piezoelectricity and flexoelectricity to the resulting polarization.

In this work, we computed the in-plane flexoelectric coefficients μ_{1111}, μ_{2222}, transverse flexoelectric coefficient μ_{3311} and out-of-plane flexoelectric coefficient μ_{3333} for monolayer MoS_2 using the charge-dipole model[59] with radial Gaussian regularization[54, 56, 60–63] enforcing charge conservation with a Lagrange multiplier and adding an ionic charge term in the definition of polarization. The significance of the missing charge term is estimated in the computation of μ_{3333}, by comparison with the simulation paper of Javvaji et al.[53] and the experimental papers of Brennan et al.[57, 58]. Our calculations illustrate that the results for this flexoelectric coefficient computed with the improved definition of polarization agree in magnitude with experimental measurements, with the possible reason causing the discrepancy in sign discussed. Moreover, two critical factors capable of affecting the sign of flexoelectric coefficient are fully elucidated while μ_{3311} is computed. Additionally, μ_{1111} and μ_{2222} are calculated by using an in-plane displacement field that effectively eliminates the piezoelectric contribution to the polarization.

This paper is organized as follows. In Sec.II we describe the Gaussian regularized charge-dipole model, our bending simulation set-ups and the computational methodology for the computation of the strain gradient. The computation of in-plane flexoelectric coefficient μ_{1111}, μ_{2222}, transverse flexoelectric coefficient μ_{3311} and out-of-plane flexoelectric coefficient μ_{3333} are presented and discussed in

Sec.III. Section IV concludes our findings.

II. METHODS

A. Principle of the method used to compute flexoelectricity coefficients

As written in the introduction, the direct flexoelectric effect describes the fact that a strain gradient in a material will cause an (additional) electric polarization of the material, because of the inhomogeneous distribution of positive and negative charge centers caused by the inhomogeneous deformation. Polarization being a vector described by a vector (first order tensor) and strain gradient a third order tensor, the supposedly linear relation between these two quantities is represented by a fourth order flexoelectricity tensor. Various conventions for the signification of the indices, leading to different matrix compressed representations, are used in the literature. We chose the one that puts the index corresponding to the polarization in first place, since we do not make use of the equivalence of the two strain indices:

$$\Delta P_i = \mu_{ijkl} G_{jkl} \tag{1}$$

where i, j, k, l are indices labeling the coordinates x, y, z or $1, 2, 3$. The Einstein implied summation convention for repeated indices is used.

Our goal is to compute values for these μ_{ijkl} coefficients. For that purpose we will use an inverse effect: when submitted to an external electric field, a dielectric material tends to deform so as to align its global dielectric polarization vector with the external field. Hence, we use various symmetric field configurations designed to deform inhomogeneously a MoS_2 monolayer, while not changing the global polarization contributions due to the dielectric susceptibility of the material or its piezoelectric properties. Then, we compute both the global polarization and the global strain gradient of the deformed structure and fit the (hopefully linear) relation between these two quantities to find the μ coefficients.

We shall therefore describe now, how we compute the global polarization and strain gradient in the monolayer.

B. Description of the charge dipole model used to compute the polarization of a monolayer MoS_2 subjected to an external electric field

We start with the regularized charge-dipole (QP) model[54, 56, 60–63], in which each atom of a MoS_2 nanoribbon is described by the combination of an effective charge and a dipole with radial Gaussian distributions, plus an effective electronegativity. The total electrostatic energy E_{elec} associated with those effective charges $\{q_\alpha\}$ and dipoles $\{\boldsymbol{p}_\alpha\}$ located at the atomic positions $\{\boldsymbol{r}_\alpha\}$ (with $\alpha = 1, ..., N$), in the presence of an external electric field $\boldsymbol{E}_{ext}$ is given by:

$$E_{elec} = \sum_{\alpha=1}^{N} q_\alpha(\chi_\alpha + V_{ext,\alpha}) - \sum_{\alpha=1}^{N} \boldsymbol{p}_\alpha \cdot \boldsymbol{E_{ext}} + \frac{1}{2}\sum_{\alpha=1}^{N}\sum_{\beta=1}^{N} q_\alpha T_{q-q}^{\alpha,\beta} q_\beta - \sum_{\alpha=1}^{N}\sum_{\beta=1}^{N} \boldsymbol{p}_\alpha \cdot \boldsymbol{T}_{p-q}^{\alpha,\beta} q_\beta - \frac{1}{2}\sum_{\alpha=1}^{N}\sum_{\beta=1}^{N} \boldsymbol{p}_\alpha \cdot \boldsymbol{T}_{p-p}^{\alpha,\beta} \cdot \boldsymbol{p}_\beta \quad (2)$$

where N stands for the number of atoms in the structure considered and χ_α is the electronegativity of the atom α, once inserted in the molecule. $V_{ext,\alpha}$ is the electrostatic potential at $\boldsymbol{r}_\alpha$ corresponding to the external electric field, which can be expressed as $-\boldsymbol{E}_{ext} \cdot \boldsymbol{r}_\alpha$ in the case of a uniform external field. T_{q-q}, $\boldsymbol{T}_{p-q}$ and $\boldsymbol{T_{p-p}}$ are interaction tensors between effective point charges or dipoles in vacuum (see equation 3), which have been convoluted with one radial Gaussian distribution per atom, of the form $\pi^{3/2}R_\alpha^3 exp(-|\boldsymbol{r} - \boldsymbol{r}_\alpha|^2/R_\alpha^2)$. This allows to take into account approximately the extension of the electronic clouds, and prevents the occurrence of divergence problems, i.e. polarization catastrophes, that can occur in simulations when two atoms are so close to each other that the approximation of an interaction between point charges or dipoles is not a good approximation

any more.[60–62, 64, 65]

$$\begin{cases} T^{\alpha\beta}_{q-q} &= \frac{1}{4\pi\epsilon_0 r_{\alpha\beta}}\mathrm{erf}\left(\frac{r_{\alpha\beta}}{\sqrt{R_\alpha^2+R_\beta^2}}\right) \\ \boldsymbol{T}^{\alpha\beta}_{p-q} &= -\boldsymbol{\nabla}_{\boldsymbol{r}_\alpha} T^{\alpha\beta}_{q-q} = -\frac{1}{4\pi\epsilon_0}\frac{\boldsymbol{r}_{\alpha\beta}}{r^3_{\alpha\beta}}\left[\mathrm{erf}\left(\frac{r_{\alpha\beta}}{\sqrt{R_\alpha^2+R_\beta^2}}\right) - \frac{2}{\sqrt{\pi}}\frac{r_{\alpha,\beta}}{\sqrt{R_\alpha^2+R_\beta^2}}\exp\left(-\frac{r^2_{\alpha\beta}}{R_\alpha^2+R_\beta^2}\right)\right] \\ \boldsymbol{T}^{\alpha\beta}_{p-p} &= -\boldsymbol{\nabla}_{\boldsymbol{r}_\beta}\otimes\boldsymbol{\nabla}_{\boldsymbol{r}_\alpha} T^{\alpha\beta}_{q-q} \\ &= \frac{1}{4\pi\epsilon_0}\left\{\frac{3\boldsymbol{r}_{\alpha\beta}\otimes\boldsymbol{r}_{\alpha\beta}-r^2_{\alpha\beta}\boldsymbol{I}}{r^5_{\alpha\beta}}\left[\mathrm{erf}\left(\frac{r_{\alpha\beta}}{\sqrt{R_\alpha^2+R_\beta^2}}\right) - \frac{2}{\sqrt{\pi}}\frac{r_{\alpha,\beta}}{\sqrt{R_\alpha^2+R_\beta^2}}\exp\left(-\frac{r^2_{\alpha,\beta}}{R_\alpha^2+R_\beta^2}\right)\right]\right. \\ &\quad \left. -\frac{4}{\sqrt{\pi}}\frac{\boldsymbol{r}_{\alpha\beta}\otimes\boldsymbol{r}_{\alpha\beta}}{r^2_{\alpha\beta}}\frac{1}{(\sqrt{R_\alpha^2+R_\beta^2})^3}\exp\left(-\frac{r^2_{\alpha\beta}}{R_\alpha^2+R_\beta^2}\right)\right\} \\ & \qquad \forall\alpha\neq\beta \end{cases} . \tag{3}$$

where $\boldsymbol{r}_{\alpha\beta} = \boldsymbol{r}_\beta - \boldsymbol{r}_\alpha$ is the vector pointing from α^{th} atom to β^{th} atom. R_α and R_β are the characteristic widths of Gaussian charge distributions for atom type α and β respectively. In the limit $\boldsymbol{r}_\alpha = \boldsymbol{r}_\beta$, the expressions of the various $T^{\alpha,\beta}$ interaction tensors in equation 3 converge to finite values (Eq. 4) related to the self-energy for each atom (atomic 'capacitance' or chemical hardness and polarizability).

$$\begin{cases} q_\alpha T^{\alpha,\alpha}_{q-q} q_\alpha = \frac{q_\alpha^2}{4\pi\epsilon_0}\frac{\sqrt{2/\pi}}{R_\alpha} \\ \boldsymbol{p}_\alpha \cdot \boldsymbol{T}^{\alpha,\alpha}_{p-q} q_\alpha = 0 \\ \boldsymbol{p}_\alpha \cdot \boldsymbol{T}^{\alpha,\alpha}_{p-p} \cdot \boldsymbol{p}_\alpha = -\frac{p_\alpha^2}{4\pi\epsilon_0}\frac{\sqrt{2/\pi}}{3R_\alpha^3}. \end{cases} \tag{4}$$

Our version of the QP model for MoS_2 possesses 8 parameters: 2 (χ and R) per kind of atoms by 4 kinds: Mo and S 'bulk' + Mo and S 'edge'. Details on this parameterization, by comparison with DFT data, are given in our previous work.[56]

The charges and dipoles at electrostatic equilibrium are then determined by minimizing the electrostatic energy (Eq. 2) using a Lagrange multiplier λ to enforce charge conservation in the nanoribbon:

$$f = E_{elec} + \lambda(\sum_{\alpha=1}^{N} q_\alpha - Q_{tot}) \tag{5}$$

This Lagrange multiplier can be physically interpreted as the chemical potential of the molecule.[61] This enforcement of charge conservation within the framework

of QP model is quite essential since it ensures that charges stay in the material in order to mimic the conditions of experimental measurements.[58] Requiring the derivative of function $f(q, \boldsymbol{p}, \lambda)$ with respect to q_α, $p_{x,\alpha}$, $p_{y,\alpha}$, $p_{z,\alpha}$ and λ to be zero will give a system of $4N + 1$ linear equations for determining the $4N + 1$ scalar unknowns (q_α, $p_{x,\alpha}$, $p_{y,\alpha}$, $p_{z,\alpha}$ and λ). These linear equations may be written in a matrix form:

$$\begin{bmatrix} T_{q-q} & \boldsymbol{T}^t_{p-q} & 1 \\ \boldsymbol{T}_{p-q} & \boldsymbol{T}_{p-p} & 0 \\ 1 & 0 & 0 \end{bmatrix} \begin{bmatrix} q \\ \boldsymbol{p} \\ \lambda \end{bmatrix} = \begin{bmatrix} -(\chi + V_{ext}) \\ -\boldsymbol{E}_{ext} \\ Q_{tot} \end{bmatrix} \tag{6}$$

where T_{q-q} is a block matrix with N rows and N columns. $\boldsymbol{T}_{p-p}$ is a block matrix with $3N$ rows and $3N$ columns. $\boldsymbol{T}_{p-q}$ is a block matrix with $3N$ rows and N columns. $\boldsymbol{T}^t_{p-q}$ is the transpose of $\boldsymbol{T}_{p-q}$. Similarly, blocks q and $-(\chi + V_{ext})$ have N rows and 1 column, while blocks $\boldsymbol{p}$ and $-\boldsymbol{E}_{ext}$ have $3N$ rows and 1 column. We note that the solution can be written in two parts as:

$$\begin{bmatrix} q \\ \boldsymbol{p} \\ \lambda \end{bmatrix} = \begin{bmatrix} T_{q-q} & \boldsymbol{T}^t_{p-q} & 1 \\ \boldsymbol{T}_{p-q} & \boldsymbol{T}_{p-p} & 0 \\ 1 & 0 & 0 \end{bmatrix}^{-1} \begin{bmatrix} -\chi \\ 0 \\ Q_{tot} \end{bmatrix} + \begin{bmatrix} T_{q-q} & \boldsymbol{T}^t_{p-q} & 1 \\ \boldsymbol{T}_{p-q} & \boldsymbol{T}_{p-p} & 0 \\ 1 & 0 & 0 \end{bmatrix}^{-1} \begin{bmatrix} -V_{ext} \\ -\boldsymbol{E}_{ext} \\ 0 \end{bmatrix} \tag{7}$$

where the first term on the right side corresponds to intrinsic charges q^0_α and dipoles $\boldsymbol{p}^0_\alpha$, i.e. charges and dipoles in the absence of any external electric field, that can however vary due to a mechanical deformation. The electronegativities χ_α uniquely determine these intrinsic charges and dipoles (given the atomic positions), independently from any external electric field $\boldsymbol{E}_{ext}$ or potential V_{ext}. For our calculations, the total charge of the nanoribbon (Q_{tot}) is set to be zero because of the fact that flexoelectricity is supposed to be an intrinsic property, therefore requiring no extra charge to appear. The second term on the right side corresponds to effective additional charges (q^{ind}_α) and dipoles (p^{ind}_α generated by the external

electric field and potential). This can be summarized under the form:

$$\begin{cases} p_x = \sum_{\alpha=1}^{N} (p_{x,\alpha}^0 + p_{x,\alpha}^{ind}) \\ p_y = \sum_{\alpha=1}^{N} (p_{y,\alpha}^0 + p_{y,\alpha}^{ind}) \\ p_z = \sum_{\alpha=1}^{N} (p_{z,\alpha}^0 + p_{z,\alpha}^{ind}) \\ q = \sum_{\alpha=1}^{N} (q_\alpha^0 + q_\alpha^{ind}) \end{cases} \tag{8}$$

In terms of the calculated dipoles $\boldsymbol{p}$ and charges q, the global polarization $\boldsymbol{P}$ for MoS_2 nanoribbon is defined as[59]:

$$\boldsymbol{P} = \frac{\sum_{\alpha=1}^{N} (q_\alpha \boldsymbol{r}_\alpha + \boldsymbol{p}_\alpha)}{V} \tag{9}$$

in which V is the volume of MoS_2 nanoribbon. A thickness of 6.5 Å is used in computing V.[66] More information on the charge dipole model for MoS_2 can be found in our previous work[56]. Note that since MoS_2 is not ferroelectric, the total contribution to polarization of the q_α^0 and $\boldsymbol{p}_\alpha^0$ is zero (verified numerically), so that Eq. 9 could be rewritten by taking into account the induced charges and dipoles only.

In order to compare with some DFT results or remove edge effects, periodic boundary conditions can be applied in the QP model by adding the contributions of periodic images in the interaction tensors, i.e. adding contributions obtained by replacing $r_{\alpha\beta}$ in Eq.3 with $r_{\alpha\beta} + L * p$ ($p \in [-k, k]$) , with L denoting the periodic length in a given direction and k being a very large integer. We verified that setting $k = 100$ in our calculation is already sufficiently large to reach convergence in the computation of in-plane flexoelectric coefficients μ_{1111}, μ_{2222} and out-of-plane flexoelectric coefficient μ_{3333}, thus eliminating edge effects.

C. Calculation of flexoelectricity coefficients

We illustrate the method we use to compute the flexoelectric coefficients on the special case of the determination of μ_{3311}.

1. *potential energy functional used for the 'structure' part*

The key of the molecular simulations is actually the interatomic potential, which is applied to describe the interaction among atoms. For single-layer MoS_2, the Stillinger-Weber many-body potential (E_{SW}) as parameterized by Wen et al[67] was very recently proven to be robust through a quantitative systematic comparison of structural and mechanical properties, as well as phonon dispersion for single-layer MoS_2 using density functional theory (DFT) and molecular statics calculations.[68] We therefore used this parameterizaton of the SW potential (E_{SW}) in our simulations, and found it very stable. Its analytical form and the values of the parameters are recalled in Supplementary material. The various MoS_2 nanoribbons we use in our simulations are thus initially relaxed by minimizing E_{SW}. This gives the undeformed configuration mentioned in the previous subsection.

To compute the deformed configurations, we removed the interactions between intrinsic charges and dipoles in E_{elec}, since they are already included in E_{SW}. We also neglected the total contribution of the interactions between intrinsic and induced charges and dipoles to keep only the total contributions of the interactions between charges and dipoles induced by the external field and potential (which we name E'_{elec}).

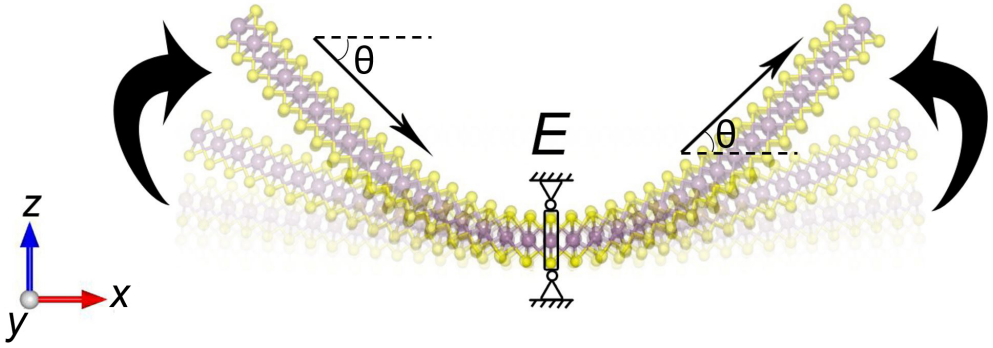

FIG. 1: Schematic of bending simulation for MoS_2 nanoribbon subjected to an external electric field. The left and right parts of the MoS_2 sheet are submitted to an electric field in the bottom-right and top-right direction, respectively. The external electric field $\boldsymbol{E}$ is represented by the arrows. θ is the angle with the $+x$ direction.

2. Initial conditions for the calculation of μ_{3311}

In order to compute μ_{3311}, a $\searrow\nearrow$-like external electric field $\boldsymbol{E}_{ext}$, with both directions of $\boldsymbol{E}_{ext}$ in the x-z plane, is applied to the MoS_2 nanoribbon, keeping the middle row of atoms fixed (as if it were attached to a virtual fixed object). This field generates a bending deformation of the nanoribbon because of the inverse flexoelectric effect, as seen in Fig 1. The conjugate gradient algorithm is then used to minimize the energy function $E_{tot} = E_{SW} + E'_{elec}$ which now includes the interactions with the external field and potential and the contributions of the effective induced charges and dipoles. The energy optimization simulation then makes the MoS_2 flake bend towards the direction of the applied electric field by adjusting the positions of the atoms until the computed average force is less than 0.00004 eV/Å. Note that all these simulations are done with a FORTRAN code that has been continuously developed in the group for years.

The mechanism of electrostatic bending of MoS_2 flake is depicted in Figure 1 of Supplementary material. We can see that negative and positive charges are shifted to opposite directions due to the non-zero transversal electric field (positive

charges move to upper left and negative ones move to top right of the MoS_2 flake). The interaction between the electric field generated by the induced charges and the external electric field produces two torques with opposite direction, termed τ_1 and τ_2, which may be expressed as $q\boldsymbol{r} \times \boldsymbol{E}_{ext}$, making the two sides of the MoS_2 flake respectively bend towards the direction of the external electric field with the fixed atoms as the rotation axis, while giving a zero total polarization along the vertical axis.

3. *Calculation of* μ_{3311}

Contributions to the polarization of a given dielectric material submitted to an external electric field may come from piezoelectricity, flexoelectricity and electric susceptibility. In the simulations defined in the previous subsection, piezoelectricity may not be taken into account due to the symmetric bending deformation[52]. This makes the total induced polarization due to the first order deformation gradient become zero. Additionally, one can find the total external electric field along the out-of-plane is also zero. Hence, the out-of-plane polarization equal to the product of the susceptibility and the electric field should be removed as well. The remaining flexoelectric part of the out-of-plane polarization P_3 can be written as:

$$P_3 = \sum_{j=1}^{3}\sum_{k=1}^{3}\sum_{l=1}^{3} \mu_{3jkl} G_{jkl} \tag{10}$$

with μ_{3jkl} standing for flexoelectric tensor components. With the setup defined in the previous section, this can be approximated by:

$$P_3 = \mu_{3311} G_{311} \tag{11}$$

Hence μ_{3311} can be determined as the slope of the supposedly linear relation between P_3 and G_{311}. Details on the computing method for determining strain gradient can be found in Supplementary material.

III. RESULTS AND DISCUSSION

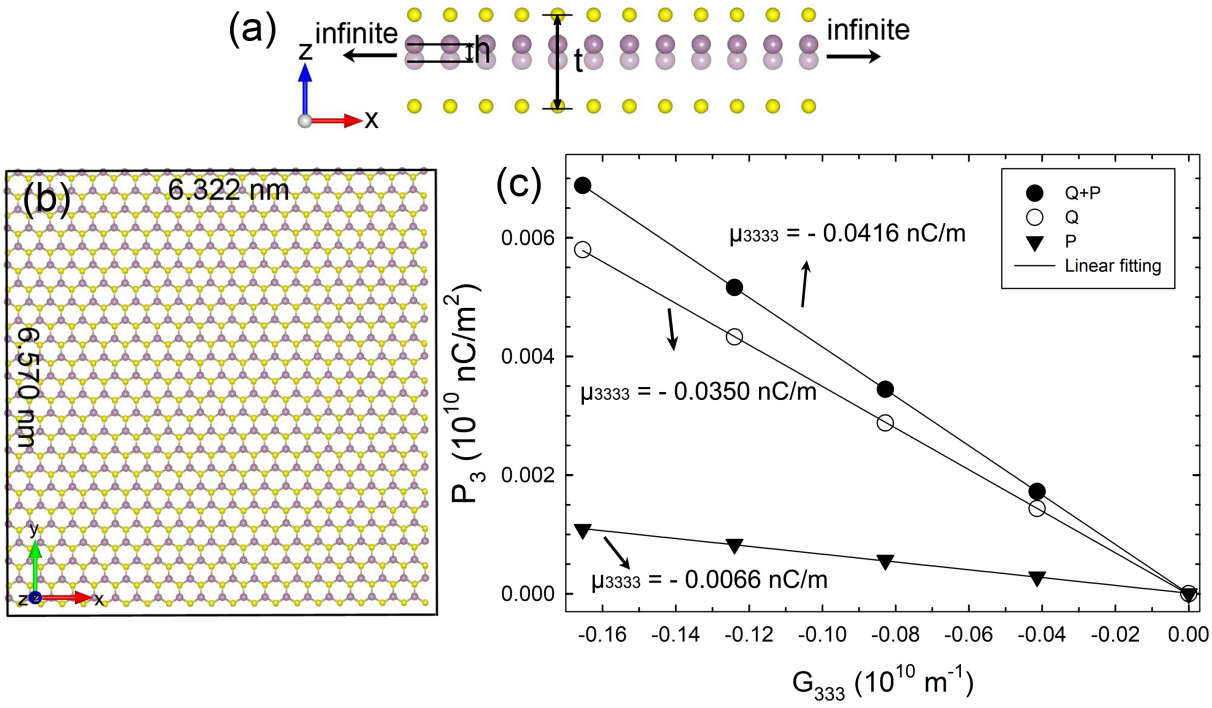

FIG. 2: (a) Schematic diagram of creation of strain gradient G_{333} inside monolayer MoS_2. h and t stand for the small upward shift for a layer of molybdenum atom and the geometric thickness of monolayer MoS_2, respectively. (b) Basic unit for periodic monolayer MoS_2, with length and width of basic unit being 6.570 nm and 6.322 nm, respectively. (c) Variation of polarization P_3 with strain gradient G_{333} for monolayer MoS_2.

In this section, we discuss the results we got for the computation of the in-plane flexoelectric coefficients μ_{1111}, μ_{2222}, the transverse flexoelectric coefficient μ_{3311} and the out-of-plane coefficient μ_{3333}. The parameters for E_{SW} and QP model used in this work were initially validated through calculation of the in-plane piezoelectric constant e_{222} for an MoS_2 monolayer. We found a value of the same order of magnitude as the corresponding experimental result (more details

are given in Supplementary material).

A. Out-of-plane flexoelectric coefficient μ_{3333}

As can be seen on Fig.2a, for this calculation, the layer of molybdenum atoms is shifted a small distance h to the positive direction of z axis to generate a strain gradient only along the out-of-plane (z) direction. In this case, the unique strain gradient that does exist is G_{333} and the expression for computing μ_{3333} can be written as $\mu_{3333} = \frac{\partial P_3}{\partial G_{333}}$. The geometric thickness of monolayer MoS_2 is t. With both h and t, the strain gradient G_{333} can be computed as $-\frac{8h}{t^2}$, which may be derived by: $G_{333} = \frac{d^2u_z(0)}{dz^2} \approx \frac{u_z(-\frac{t}{2})+u_z(\frac{t}{2})-2u_z(0)}{(t/2)^2} = \frac{0+0-2h}{(t/2)^2} = -\frac{8h}{t^2}$, with $u_z(\frac{t}{2})$, $u_z(-\frac{t}{2})$ and $u_z(0)$ representing the displacement of atoms for top sulfur layer, bottom sulfur layer and molybdenum layer, respectively. In this calculation, we enforce periodic boundary conditions to eliminate edge effects that can be quite important in such a setup. As can be seen on Fig.2b, we use a MoS_2 flake with a width of 6.164 nm and a length of 6.388 nm as supercell, which gives periods along x and y direction of 6.322 nm and 6.570 nm, respectively. Bond length between Mo and S is set as 2.39763 Å in the presence of periodic boundary conditions. On Fig.2c, we plot the polarization P_3 as a function of G_{333}, in order to obtain the flexoelectric coefficient μ_{3333} of 2D MoS_2. Three different ways to compute the polarization are used (using $q_\alpha \boldsymbol{r}_\alpha$ only, using $\boldsymbol{p}_\alpha$ only or using both terms in Eq.9, with charges and dipoles computed using the QP scheme in the three cases). The units of polarization P_3 and strain gradient G_{333} are converted from e/Å^2 and Å^{-1} to 10^{10} nC/m^2 and 10^{10} m^{-1} respectively, so as to readily obtain μ_{3333} in nC/m from the slope of the fitted straight line. We compare μ_{3333} computed under the various definitions of polarization with that obtained from the experimental measurements conducted by Brennan et al in 2017 and 2020[57, 58], respectively, as shown in Table I.

TABLE I: Comparison between out-of-plane flexoelectric coefficients μ_{3333} obtained by charge-dipole model and experimental measurements. The two different contributions to the polarization coming from charges alone or dipoles alone are considered separately then together for the computation of μ_{3333} by the charge-dipole model.

Ref.	μ_{3333} (nC/m)	Definition of polarization
present work	-0.0416	$P_3 = \frac{\sum_{\alpha=1}^{N}(q_\alpha r_{3,\alpha}+p_{3,\alpha})}{V}$
present work	-0.0350	$P_3 = \frac{\sum_{\alpha=1}^{N} q_\alpha r_{3,\alpha}}{V}$
present work	-0.0066	$P_3 = \frac{\sum_{\alpha=1}^{N} p_{3,\alpha}}{V}$
Brennan et al (2017)[57]	0.08 or 0.12	———
Brennan et al (2020)[58]	0.065	———

It can be seen that the result for μ_{3333} computed when the charge term is included in the definition of polarization will be comparatively closer to the experimental result in absolute value whereas μ_{3333} computed with the dipole term only considered is of the same order of magnitude but much smaller than the experimental value. This manifests that the charge term, omitted/neglected in Ref.[52], cannot be neglected for the calculation of polarization for MoS_2. We do not take into account the discrepancy in sign between our computed results and the results of the Piezoresponse Force Microscopy (PFM) measurements of Brennan et al., since we believe that it is due to a problem of different definition for the algebraic (or not) radius of curvature. This is reflected in another experimental measurements of out-of-plane flexoelectric coefficient μ_{3333} for few-layers MoS_2 with PFM, very recently conducted by Hirakata et al[69]. In their work, the sign of the out-of-plane flexoelectric coefficient is measured to be negative, though they quote a positive number. Indeed, using their Eq. 9, one can get $\mu_{3333} = \mu_{39} = -c_{33}\epsilon_3/\frac{\partial E_3}{\partial x_3}$. S-

ince c_{33}, ϵ_3 and $\frac{\partial E_3}{\partial x_3}$ (see their Figure 11) are all positive, their μ_{3333} is in fact negative.[69]

Other problems could arise because the MoS_2 samples used in the PFM experiments might not be as perfect as that used in our calculation. Indeed, intrinsic atomic defects have been observed in the CVD-grown monolayer MoS_2 using near-field photoluminescence imaging[70]. These defects could give rise to very localized strain gradients and therefore to noticeable additional polarization due to flexoelectricity, since monolayer MoS_2 is sensitive to any tiny deformation along vertical direction (z) due to its atomically thin thickness. Furthermore, the possibly existing interfacial contamination between substrate and MoS_2 sample and the other uncertainties relevant to the measurements could be another cause of discrepancy between our theoretical results and the experimental ones. It would be useful if these (difficult) experiments could be repeated many times, so as to reduce the large uncertainties on the experimental results, but we feel that our present results for μ_{3333} of a MoS_2 monolayer, agree well enough with experiment, to encourage us to compute other flexoelectric coefficients for MoS_2 monolayer, for which we do not have experimental data to compare with.

B. Transverse flexoelectric coefficient μ_{3311}

The bending simulation described in the 'Methods' section is employed to compute the transverse flexoelectric coefficient μ_{3311} of MoS_2. Since the visible displacements are mostly along z direction, the strain gradient enabling polarization to be nonzero is principally G_{311}. Hence, μ_{3311} may be approximately expressed as $\mu_{3311} = \frac{\partial P_3}{\partial G_{311}}$. Fig.3a presents the variations of the out-of-plane polarization P_3 for a MoS_2 flake bent along (x) zigzag direction with respect to the strain gradient G_{311}. One can notice that the intercept of the linear-fitting straight line is almost zero, meaning that the nonzero polarization is mainly caused by G_{311}.

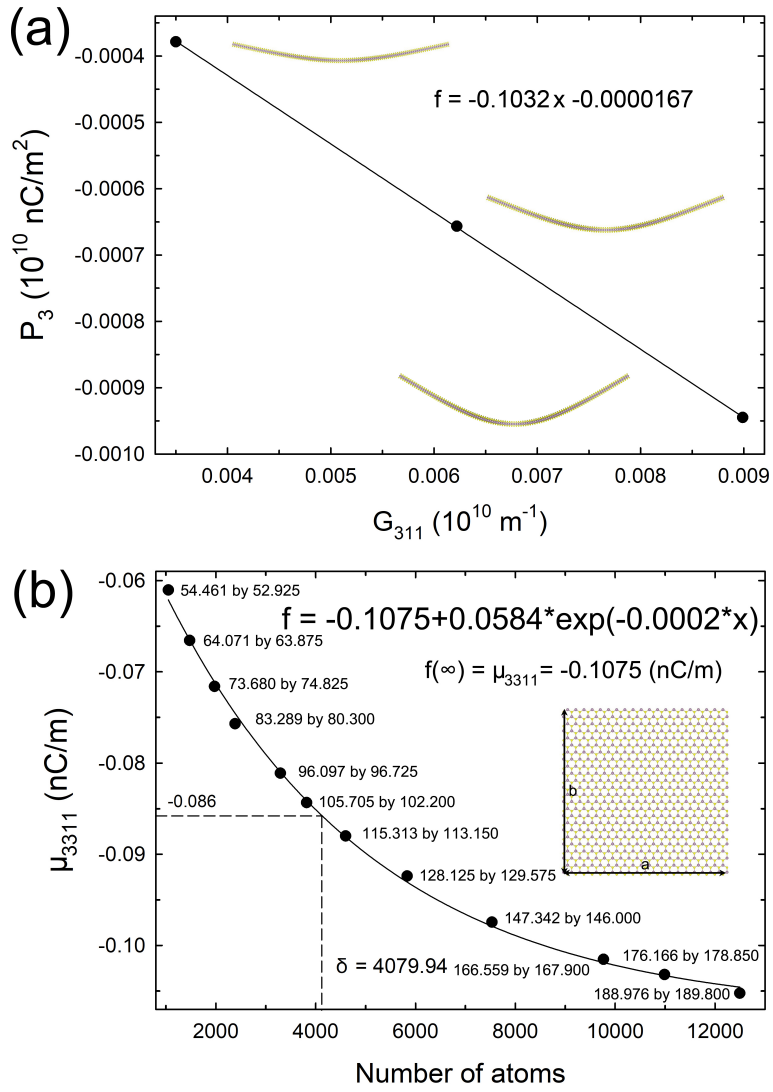

FIG. 3: (a)Variation of P_3 with strain gradient G_{311}. The magnitude of the electric fields imposed to the MoS_2 monolayer for bending simulation are 0.0424 V/Å, 0.0566 V/Å, 0.0707 V/Å, respectively. (b)Transverse flexoelectric coefficient μ_{3311} vs number of atoms. An exponential function is used to describe the tendency to convergence. The lengths a and b of the sides the of MoS_2 flakes are marked next to each computed μ_{3311}. The first and second number for the size of MoS_2 flake corresponds to a and b, respectively. The unit of a and b is Å. δ denotes characteristic length of exponential function. The angle between the electric field and the positive direction of the x-axis is set to 45 degrees.

Contrarily to what we did for the computation of μ_{3333}, periodic boundary conditions cannot be exerted in the bending simulation because bending of material submitted to the external electric field will break the periodicity of the lattice itself. We therefore studied the effect of the size of the MoS_2 flake, on the computed flexoelectric coefficient. Fig.3b is plotted to present the variation of transverse flexoelectric coefficient μ_{3311} with the increasing number of atoms. It can be seen that the value of μ_{3311} scales non-linearly down with the number of atoms. The larger the number of atoms, the more obvious the trend of curve convergence. To obtain a converged value, data is fitted with an exponential function. With the number of atoms increasing, the transverse flexoelectric coefficient μ_{3311} converges to -0.1075 nC/m, comparable to that for phosphorene[47] and boron nitride sheet[48]. A comparison is made between μ_{3311} computed with QP model and that obtained by DFT-based first principle calculation by Shashikant et al[51], as listed in Table II. It can be seen that our computed result for μ_{3311} agrees much better in absolute value with that obtained from DFT calculations than the one computed by Zhuang et al.[52], signifying that the computation of transverse flexoelectric coefficient of MoS_2 can be well captured by the QP model, if the proper definition for the polarization is used. Note that the radial polarization $\boldsymbol{p}_r$ defined in reference [51] and [71] to compute μ_{3311} can be considered equivalent to the p_z used in our work, since it is always locally perpendicular to the 2D material. We will now turn again to the question of the sign of the flexoelectric coefficients.

Understanding the reason causing the discrepancy in the sign of flexoelectric coefficients is essential because the direction of the electric polarization induced by flexoelectricity is of significance for sensors and energy harvesters. We will study successively the sign of the polarization and the strain gradient.

Concerning polarization, we separate two distinct contributions: one due to the deformation of the lattice and the other one due to charge transfer between the inner and outer layers during bending. For that purpose we first compute

TABLE II: Comparison between transverse flexoelectric coefficient μ_{3311} obtained by charge dipole model and theoretical computation.

Ref.	μ_{3311} (nC/m)
present work	-0.1075
Shashikant et al [51]	0.14
Zhuang et al [52]	0.032

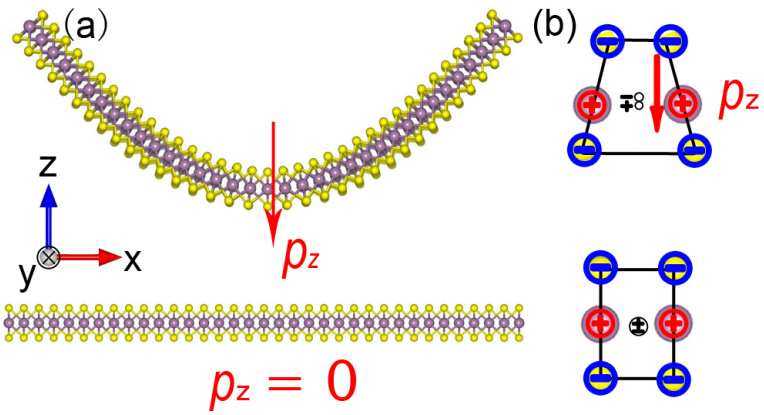

FIG. 4: Origin of flexoelectric effect in bending deformation. (a) Under bending deformation, the direction of induced dipole moment points to -z direction. For an undeformed MoS_2 flake, the total dipole moment along the direction normal to the surface of MoS_2 is zero. (b) Separation of the centers (in black) of positive (in red) and negative charges (in blue) due to bending deformation.

the relaxed positions of a MoS_2 flake deformed under the action of an electric field, using the QP model (Fig.4a). Then we compute the polarization for that bent MoS_2 flake, for an hypothetical case where the charges of the sulfur atoms would be the same in the upper and lower layers. In that hypothetical case, the computation gives a polarization in the negative direction of z axis, whereas in the undeformed MoS_2 flake, the total dipole moment along the out-of-plane direction

is always zero due to the fact that the molybdenum atomic layer is equidistantly sandwiched between two layers of sulfur atoms. Fig.4b illustrates this phenomenon with the case of the two rows of atoms nearest to the symmetry plane of the deformed flake: the molybdenum cations are repelled away from the inner part of the bend (which is its denser part). The consequence is that, while the charge center of the sulfur anions stays half way between the two layers, the charge center of the molybdenum is lower which results in a polarization pointing downwards (hence a negative contribution to μ_{3311} since G_{311} is positive in that case).

However, the above effect is not enough to fully account for the polarization since we artificially used identical charges for the sulfur atoms. in reality, since the overlapping of the electronic clouds of two nearby ions change during bending, partial charges can be transferred from one sulfur layer to the other. In order to understand that second contribution to the polarization, two representative areas of the same deformed MoS_2 flake, named A and B, are considered in Fig.5a. The average charge for the sulfur atoms in the upper and lower layers, calculated by averaging net charges obtained by the QP model along y direction perpendicular to the figure, are $-0.776\ e$ and $-0.803\ e$, respectively. Therefore the atoms of the lower sulfur layer appear to be more negative than those of the upper layer. This creates a net dipole moment pointing from the outside to the inside of the curvature (in the positive direction of z axis in our case). At the B site, the curvature is much smaller than at the A site and consequently the difference in charges between sulfur atoms in the upper and lower layer is smaller. In Fig.5b, we plotted the average charge difference $\Delta q = q_{lower} - q_{upper}$ between sulfur atoms in the lower and upper layer, as a function of their index along the x coordinate (see numbers on the molecular picture inside the graph). It can be seen that the absolute value of Δq decreases with the increasing index of sulfur, which agrees with what we expected before implementing the computation, since it corresponds to the flexoelectric effect: if the strain gradient is smaller, then the polarization is smaller (in absolute

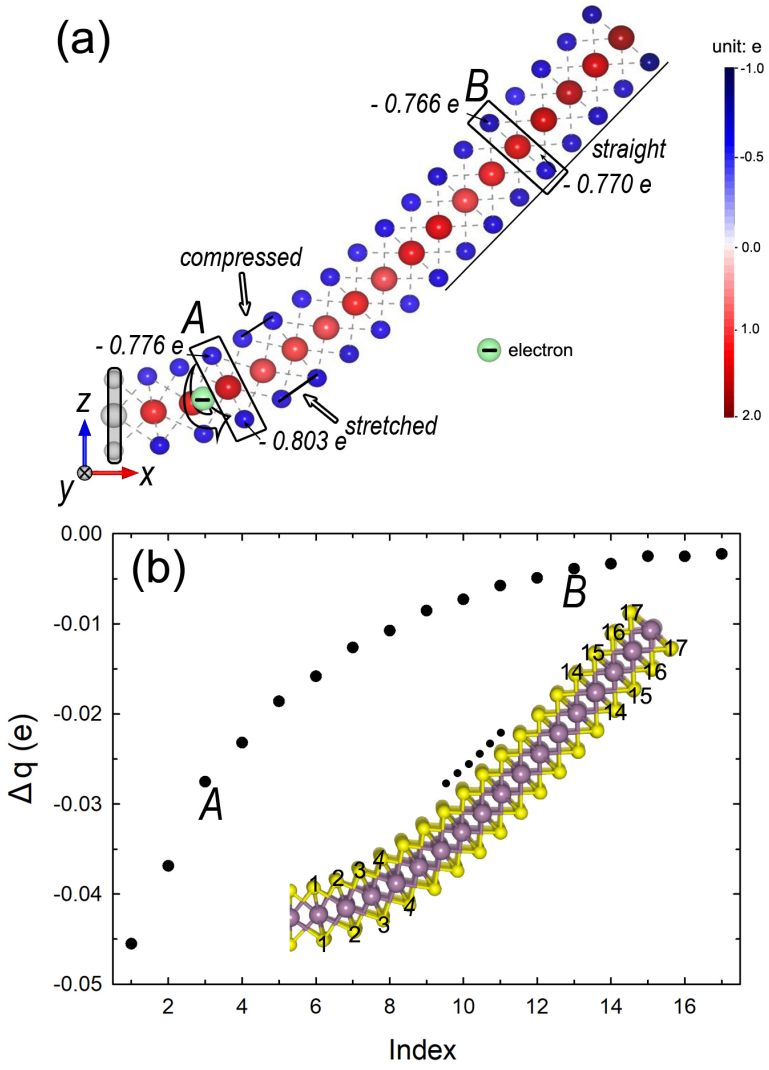

FIG. 5: (a) Charge distribution of a bent MoS_2 subjected to $E_x = E_z = 0.4$ V/Å. A and B are two representative regions for explanation of charges transfer from the upper layer to the lower layer, respectively. (b) Δq vs index. Δq is calculated as the charge of sulfur atoms in the lower layer minus the corresponding quantity for the upper layer. The upper and lower sulfur atoms are numbered by increasing value of z. Only the right portion of the bent MoS_2 is shown here.

value). Hence, we have two contributions in opposite directions: a downward electric dipole moment due to bending of the lattice and an upward electric dipole moment due to charge transfer. In the case of MoS_2, our computations show that polarization caused by bending deformation of lattice (which tends to give a negative flexoelectric coefficient) surpasses that resulting from charge transfer (which tends to give a positive flexoelectric coefficient). It is worth mentioning here that a negative μ_{3311} for MoS_2 monolayer has very recently been obtained using first-principles linear-response theory[71]. Very interestingly, it can be found in their calculations that two contributions coming from the dipolar and the lattice-mediated response, respectively, to the total polarization response also play a competing role, the signs of the former and the latter tending to be opposite, as in our study.

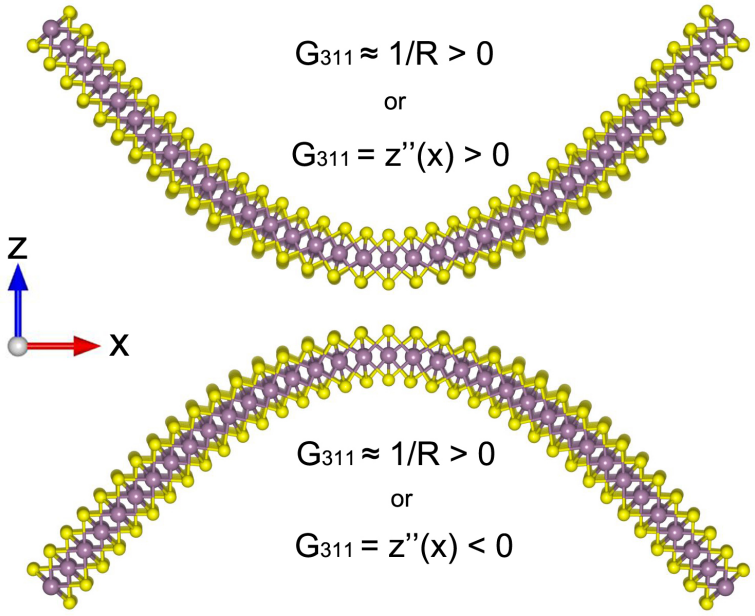

FIG. 6: Illustration of the different definitions for strain gradient G_{311}.

We now turn to the sign of the strain gradient. In a review paper, Wang et al[72] pointed the discrepancies between definitions and symbols of physical

quantities to be one of the reasons for the inconsistency of the reported signs of flexoelectric coefficients. It is often the case for the strain gradient G_{311}. Indeed, on Fig.6 we illustrate that the strain gradient, defined as $G_{311} = u_z''(x)$ which can be either positive or negative, is often approximated as the inverse of the radius of curvature. Since, for some authors, the radius of curvature is always positive, G_{311} is always positive for them, regardless of the bending direction of the material. Slightly differently, Kundalwal et al[48] considered a boron nitride sheet shaped as an upward convex curved arch and defined G_{311} as the absolute value of the inverse of radius of curvature. We note, however, that we used a downward pointing bend (top part of Fig.6 and Fig.4) which gives a positive strain gradient for all these definitions.

The previous considerations tentatively explain why flexoelectric coefficients can be either positive or negative, due to a competition between lattice and charge transfer effect, and not always positive as some authors define it by using absolute values inside their definition.

C. In-plane flexoelectric coefficient μ_{1111} and μ_{2222}

Inspired by the work of Hong et al[73], the in-plane flexoelectric coefficients μ_{1111} and μ_{2222} are computed in the present work. Strain gradient G_{111} is created by displacing every atoms along x axis, according to a parabolic displacement function $u_x(x)$. Fig.7a is a schematic diagram showing the transverse displacement of atoms for a MoS_2 flake with a bigger (so that it be visible thanks to the two vertical lines) strain gradient imposed along x axis. Fig.7b shows the variation of displacement of atoms along x direction in the case $\Delta d = u_x(x) = 0.01 - 10^{-5}x^2$, strain ϵ_{xx} and strain gradient $\epsilon_{xx,x}$ (G_{111}) as functions of the position along x axis for MoS_2. We can see that the total strain is zero due to the symmetric distribution of displacement with respect to $x = 0$. Hence, the polarization due

to piezoelectricity can be fully removed from the total polarization, leaving only flexoelectricity. Furthermore, μ_{1111} can be expressed as $\mu_{1111} = \frac{\partial P_1}{\partial G_{111}}$ and for a similar simulations with parabolic displacement along y, $\mu_{2222} = \frac{\partial P_2}{\partial G_{222}}$. The magnitude of strain gradient for our calculations of μ_{1111} and μ_{2222} ranges from 0 to 0.00004 Å^{-1}, which is small enough to neglect any non-linear effect.

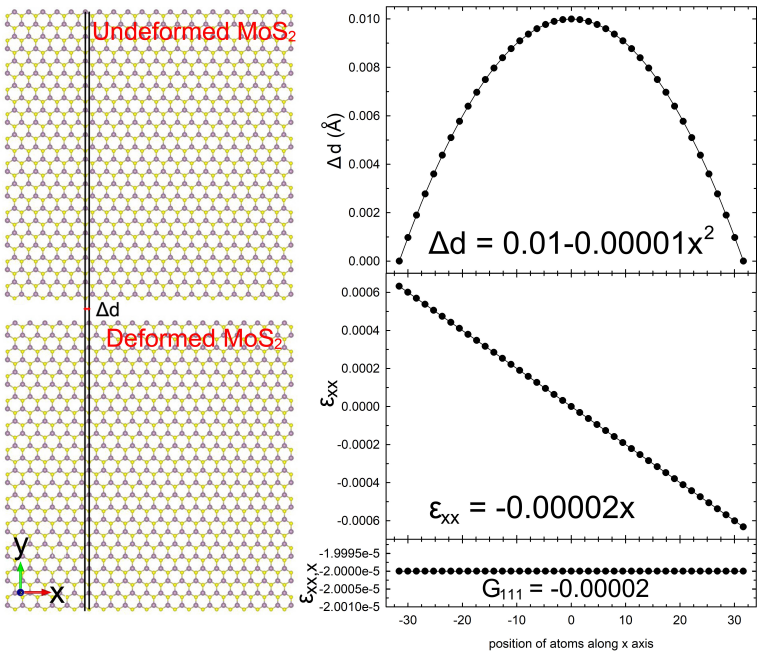

FIG. 7: (a) Applied displacement field along x axis for each atom with Δd denoting the difference between the x coordinate of atoms in deformed MoS_2 and that in undeformed MoS_2. The two vertical lines are guides to the eye to see the displacements along x between the top and bottom sub-figures. (b) Displacement field $\Delta d = u_x(x)$, strain (ϵ_{xx}) and strain gradient ($\epsilon_{xx,x} = G_{111}$) vs the position along x axis for MoS_2.

The dependence of in-plane flexoelectric coefficients μ_{1111} and μ_{2222} on the width of nanoribbon with infinite lengths is shown in Figure 4 in Supplementary material. Clearly, the in-plane flexoelectric coefficients increase as the width of nanoribbons increases (polynomial fits are guides to the eye). The non-convergence behavior of those flexoelectric coefficients with the increase of the width of the nanoribbons has

been elaborately discussed[74]. Hao et al. reveals through DFT calculations that the flexoelectric coefficients of the 2D Janus TMDs nanoribbons depend strongly upon their widths. The (slightly) different results for the two orientations are probably due to edge effects different for armchair and zigzag edges. To completely eliminate edge effect we use periodic boundary conditions in both directions for the displacements. In their article,[73] Hong et al. computed the in-plane flexoelectric coefficients of $SrTiO_3$ using a strain gradient with a cosine form, to be compatible with the periodic boundary conditions. In our work, strain gradient is a constant function (see Fig.7b), which is an even simpler case. Fig.8 shows the variations of polarization P_1 and P_2 with strain gradient G_{111} and G_{222} for those doubly-periodic setups. The computed flexoelectric coefficients μ_{1111} and μ_{2222} are 0.6872 nC/m and 0.7119 nC/m, respectively. Hence, the in-plane flexoelectric properties of doubly-infinite MoS_2 are nearly isotropic, i.e. independent of the zigzag or armchair direction.

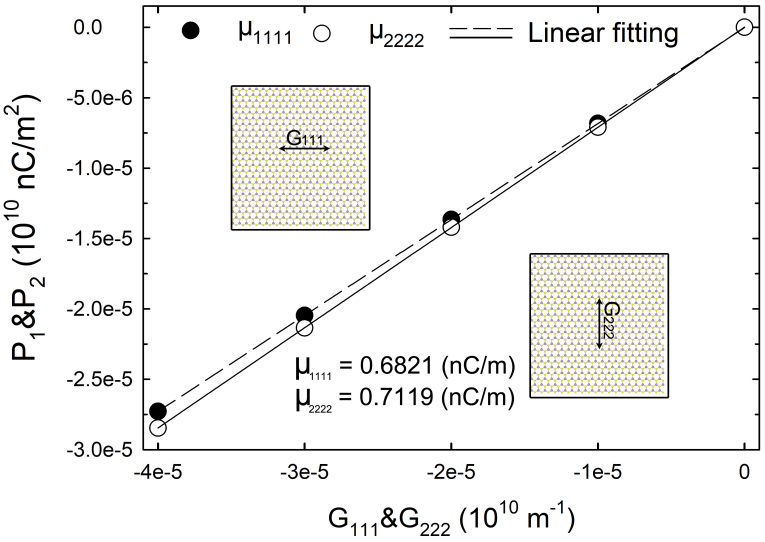

FIG. 8: Variations of polarization P_1 and P_2 with strain gradient G_{111} and G_{222}, respectively. The rectangular frame surrounding the edge of molybdenum disulfide represents the enforcement of periodic boundary conditions in both directions.

IV. CONCLUSIONS

Employing three different simulation setups, we calculated in-plane flexoelectric coefficients μ_{1111}, μ_{2222}, transverse flexoelectric coefficient μ_{3311} and out of plane flexoelectric coefficient μ_{3333} for monolayer MoS_2 using the charge dipole model and charge conservation. The out-of-plane flexoelectric coefficient μ_{3333} and transverse flexoelectric coefficient μ_{3311} computed by the charge-dipole model are compared with those obtained by experimental measurements and DFT-based first principle calculations, by which good agreement in absolute value can be seen when the charge term is included in the computation of the polarization. We discuss in details possible origins of discrepancy in sign between our calculated flexoelectric coefficient μ_{3311} and other reported results, by showing two opposite effects for the sign of the polarization. Furthermore, we emphasize that comparison of flexoelectric coefficients between different computational works requires a careful check for the sign of strain gradient and the way of defining the polarization. Concerning the computed in-plane flexoelectric coefficient μ_{1111} and μ_{2222} are found to be quasi identical, which is consistent with the analysis of symmetry for the flexoelectric coefficient tensor of a 2D continuum.

Finally, it is worth pointing out that the computed in-plane flexoelectric coefficient is about twenty times greater than out-of-plane flexoelectric coefficient for MoS_2, which can be ascribed to the fact that the net charges induced by in-plane strain gradient between every primitive cells lead to the generation of larger electric dipole moments, whereas the movement of the charge in the out-of-plane direction is restricted due to the finite thickness. Hence, a relatively small polarization is then induced in the out-of-plane direction. For 2D materials, bending seems to be the easiest way to externally generate a big strain gradient at nanoscale, on a large area. Therefore, even if in-plane flexoelectric coefficients may play a role in some systems, the differences between in-plane, out-of-plane and transverse coefficients in MoS_2 flakes is not big enough to compensate for the bigger and more

homogenous strain gradient that can be realized by bending. It is thus important to find 2D materials that optimize the transverse flexoelectric coefficients μ_{3311} for applications in energy harvesting.

V. ACKNOWLEDGMENTS

This work was supported by the EIPHI Graduate School (contract "ANR-17-EURE-0002") and the Region of Bourgogne Franche-Comté (contract 2018-0054 “ACTION μMecatro. Computations have been performed on the supercomputer facilities of the Mésocentre de calcul de Franche-Comté.

VI. DATA AVAILABILITY

The data that support the findings of this study are available from the corresponding author upon reasonable request.

---

[1] P. V. Yudin and A. K. Tagantsev, Nanotechnology **24**, 432001 (2013).

[2] Q. Deng, M. Kammoun, A. Erturk, and P. Sharma, Int. J. Solids Struct. **51**, 3218 (2014).

[3] K. F. Wang and B. L. Wang, Int. J. Eng. Sci. **116**, 88 (2017).

[4] S. Zhang, K. Liu, M. Xu, and S. Shen, Appl. Phys. Lett. **111**, 082904 (2017).

[5] U. K. Bhaskar, N. Banerjee, A. Abdollahi, Z. Wang, D. G. Schlom, G. Rijnders, and G. Catalan, Nat. Nanotechnol. **11**, 263 (2016).

[6] G. Dong, S. Li, M. Yao, Z. Zhou, Y.-Q. Zhang, X. Han, Z. Luo, J. Yao, B. Peng, Z. Hu, et al., Science **366**, 475 (2019).

[7] W. Huang, X. Yan, S. R. Kwon, S. Zhang, F.-G. Yuan, and X. Jiang, Appl. Phys. Lett. **101**, 252903 (2012).

[8] S. Zhang, M. Xu, K. Liu, and S. Shen, J. Phys. D: Appl. Phys. **48**, 485502 (2015).

[9] V. S. Mashkevich and K. B. Tolpygo, Sov. Phys. JETP **5**, 435 (1957).

[10] S. M. Kogan, Sov. Phys.-Solid State **5**, 2069 (1964).

[11] V. L. Indenbom, E. B. Loginov, and M. A. Osipov, Kristallografiya **26**, 1157 (1981).

[12] V. L. Indenbom, E. B. Loginov, and M. A. Osipov, Sov Phys - Crystallogr. **26**, 656 (1981).

[13] A. K. Tagantsev, Zh. Eksp. Teor. Fiz. **88**, 2108 (1985).

[14] A. K. Tagantsev, Phys. Rev. B **34**, 5883 (1986).

[15] E. Sahin and S. Dost, Int. J. Eng. Sci. **26**, 1231 (1988).

[16] P. Harris, J. Appl. Phys. **36**, 739 (1965).

[17] A. Askar, P. C. Y. Lee, and A. S. Cakmak, Phys. Rev. B **1**, 3525 (1970).

[18] R. Maranganti and P. Sharma, Physical Review B **80**, 054109 (2009).

[19] R. Resta, Phys. Rev. Lett. **105**, 127601 (2010).

[20] T. Dumitrică, C. M. Landis, and B. I. Yakobson, Chem. Phys. Lett. **360**, 182 (2002).

[21] S. V. Kalinin and V. Meunier, Phys. Rev. B **77**, 033403 (2008).

[22] I. Naumov, A. M. Bratkovsky, and V. Ranjan, Phys. Rev. Lett. **102**, 217601 (2009).

[23] P. J. Mitchell and D. Fincham, J. Phys. Condens. Matter **5**, 1031 (1993).

[24] M. S. Majdoub, P. Sharma, and T. Cagin, Phys. Rev. B **77**, 125424 (2008).

[25] R. Mbarki, J. B. Haskins, A. Kinaci, and T. Cagin, Phys. Lett. A **378**, 2181 (2014).

[26] A. Chatzopoulos, P. Beck, J. Roth, and H.-R. Trebin, Phys. Rev. B **93**, 024105 (2016).

[27] S. Mao, P. K. Purohit, and N. Aravas, Proc. R. Soc. A: Math. Phys. Eng. Sci. **472**, 20150879 (2016).

[28] Y. Mao, S. Ai, X. Xiang, and C. Chen, Appl. Math. Model **40**, 7115 (2016).

[29] H. T. Chen, A. K. Soh, and Y. Ni, Acta Mech. **225**, 1323 (2014).

[30] Q. Li, C. T. Nelson, S.-L. Hsu, A. R. Damodaran, L.-L. Li, A. K. Yadav, M. McCarter, L. W. Martin, R. Ramesh, and S. V. Kalinin, Nat. Commun. **8**, 1 (2017).

[31] K. M. Hamdia, H. Ghasemi, X. Zhuang, N. Alajlan, and T. Rabczuk, Comput. Mater. Contin. **59**, 79 (2019).

[32] L. Xiang, X. Zeng, X. Huang, and G. Li, Phys. Lett. A **384**, 126217 (2020).

[33] H. Ghasemi, H. S. Park, and T. Rabczuk, Computer Methods in Applied Mechanics and Engineering **332**, 47 (2018).

[34] H. V. Do, T. Lahmer, X. Zhuang, N. Alajlan, H. Nguyen-Xuan, and T. Rabczuk, Computers & Structures **214**, 1 (2019).

[35] W. Ma and L. E. Cross, Appl. Phys. Lett. **79**, 4420 (2001).

[36] W. Ma and L. E. Cross, Appl. Phys. Lett. **78**, 2920 (2001).

[37] W. Ma and L. E. Cross, Appl. Phys. Lett. **81**, 3440 (2002).

[38] W. Ma and L. E. Cross, Appl. Phys. Lett. **82**, 3293 (2003).

[39] W. Ma and L. E. Cross, Appl. Phys. Lett. **86**, 072905 (2005).

[40] W. Ma and L. E. Cross, Appl. Phys. Lett. **88**, 232902 (2006).

[41] J. Narvaez and G. Catalan, Appl. Phys. Lett. **104**, 162903 (2014).

[42] L. Shu, W. Huang, S. Ryung Kwon, Z. Wang, F. Li, X. Wei, S. Zhang, M. Lanagan, X. Yao, and X. Jiang, Appl. Phys. Lett. **104**, 232902 (2014).

[43] W. Huang, K. Kim, S. Zhang, F.-G. Yuan, and X. Jiang, Phys. Status. Solidi. Rapid. Res. Lett. **5**, 350 (2011).

[44] A. Kvashnin, P. Sorokin, and B. Yakobson, J. Phys. Chem. Lett. **6**, 2740 (2015).

[45] S. Chandratre and P. Sharma, Appl. Phys. Lett. **100**, 023114 (2012).

[46] S. I. Kundalwal, S. A. Meguid, and G. J. Weng, Carbon **117**, 462 (2017).

[47] T. Pandey, L. Covaci, M. V. Milošević, and F. M. Peeters, Phys. Rev. B **103**, 235406 (2021).

[48] S. I. Kundalwal, V. K. Choyal, and V. Choyal, Acta Mech. **232**, 3781 (2021).

[49] W. Shi, Y. Guo, Z. Zhang, and W. Guo, J. Phys. Chem. Lett. **9**, 6841 (2018).

[50] W. Shi, Y. Guo, Z. Zhang, and W. Guo, J. Phys. Chem. C **123**, 24988 (2019).

[51] S. Kumar, D. Codony, I. Arias, and P. Suryanarayana, Nanoscale **13**, 1600 (2021).

[52] X. Zhuang, B. He, B. Javvaji, and H. S. Park, Phys. Rev. B **99**, 054105 (2019).

[53] B. Javvaji, B. He, X. Zhuang, and H. S. Park, Phys. Rev. Mater. **3**, 125402 (2019).

[54] Z. Wang and M. Devel, Phys. Rev. B **76**, 195434 (2007).

[55] Z. Wang, M. Zdrojek, T. Mélin, and M. Devel, Phys. Rev. B **78**, 085425 (2008).

[56] Y. Yang, M. Devel, and Z. Wang, J. Chem. Phys. **149**, 124102 (7) (2018).

[57] C. J. Brennan, R. Ghosh, K. Koul, S. K. Banerjee, N. Lu, and E. T. Yu, Nano Lett. **17**, 5464 (2017).

[58] C. J. Brennan, K. Koul, N. Lu, and E. T. Yu, Appl. Phys. Lett. **116**, 053101 (2020).

[59] M. L. Olson and K. R. Sundberg, J. Chem. Phys. **69**, 5400 (1978).

[60] A. Mayer, P. Lambin, and R. Langlet, Appl. Phys. Lett. **89**, 063117 (2006).

[61] A. Mayer, Phys. Rev. B **75**, 045407 (2007).

[62] A. Mayer and P.-O. Åstrand, J. Phys. Chem. A **112**, 1277 (2008).

[63] A. Mayer, A. L. Gonzalez, C. M. Aikens, and G. C. Schatz, Nanotechnology **20**, 195204 (2009).

[64] L. Jensen, P. O. Åstrand, A. Osted, J. Kongsted, and K. V. Mikkelsen, J. Chem. Phys. **116**, 4001 (2002).

[65] R. Langlet, M. Devel, and P. Lambin, Carbon **44**, 2883 (2006).

[66] X. Li and H. Zhu, J. Materiomics **1**, 33 (2015).

[67] M. Wen, S. N. Shirodkar, P. Plecháč, E. Kaxiras, R. S. Elliott, and E. B. Tadmor, J. Appl. Phys. **122**, 244301 (2017).

[68] M. Madziarz, Materials **14**, 519 (2021).

[69] H. Hirakata, Y. Fukuda, and T. Shimada, J. Phys. D: Appl. Phys. **55**, 125302 (2021).

[70] Y. Lee, S. Park, H. Kim, G. H. Han, Y. H. Lee, and J. Kim, Nanoscale **7**, 11909 (2015).

[71] M. Springolo, M. Royo, and M. Stengel, Phys. Rev. lett. **127**, 216801 (2021).

[72] B. Wang, Y. Gu, S. Zhang, and L.-Q. Chen, Prog. Mater. Sci **106**, 100570 (2019).

[73] J. Hong, G. Catalan, J. F. Scott, and E. Artacho, J. Phys. Condens. Matter **22**,

112201 (2010).

[74] W. Hao, Z. Wu, X. Li, and Y. Pu, J. Appl. Phys. **129**, 185101 (2021).